**Theoret. Appl. Mech.**, Vol.39, No.4, pp. 365–390, Belgrade 2012

# Homotopy simulation of axisymmetric laminar mixed convection nanofluid boundary layer flow over a vertical cylinder

**M.M.Rashidi*** **O.Anwar Bég†**
**N.Freidooni Mehr ‡** **A.Hosseini §** **R.S.R.Gorla ¶**

**Abstract**

In this paper, the semi-analytical/numerical technique known as the homotopy analysis method (*HAM*) is employed to derive solutions for the laminar axisymmetric mixed convection boundary-layer nanofluid flow past a vertical cylinder. The similarity solutions are employed to transform the parabolic partial differential conservation equations into system of nonlinear, coupled ordinary differential equations, subject to appropriate boundary conditions. A comparison has been done to verify the obtained results with the *purely numerical* results of Grosan and Pop (2011) with excellent correlation achieved. The effects of nanoparticle volume fraction, curvature parameter and mixed convection or buoyancy parameter on the dimensionless velocity and temperature distributions, skin friction and wall temperature gradients are illustrated graphically. HAM is found to demonstrate excellent potential for simulating nanofluid dynamics problems. Applications of the study include materials processing and also thermal enhancement of energy systems.

**Keywords**: Semi-analytical solution; mixed convection; boundary-layers; vertical cylinder; nanofluid; HAM; auxiliary parameter; energy systems enhancement.

*Mechanical Engineering Department, Engineering Faculty of Bu-AliSina University, Hamedan,Iran

†Gort Engovation Research (Propulsion/Biomechanics), 15 Southmere Ave., Bradford, BD73NU, England,e-mail: gortoab@gmail.com

‡Young Researchers Club & Elites, Hamedan Branch, Islamic Azad University, Hamedan, Iran

§Mechanical Engineering Department, Engineering Faculty of Bu-AliSina University, Hamedan,Iran

¶Department of Mechanical Engineering, Cleveland State University, Ohio, USA

**Nomenclature**

$a$ - radius of cylinder
$C_f$ - skin friction coefficient
$c_i$ - arbitrary constant
$C_p$ - specific heat at constant pressure
$g$ - acceleration due to gravity
$Gr$ - Grashof number
$\hbar$ - auxiliary nonzero parameter
$\mathcal{H}$ - auxiliary function
$k$ - heat transfer coefficient
$l$ - characteristic length of the cylinder
$\mathcal{L}$ - auxiliary linear operator
$\mathcal{N}$ - nonlinear operator
$Nu$ - Nusselt number
$p$ - embedding parameter
Pr - Prandtl number
$q_w$ - heat flux from the surface of the cylinder
$r$ - radial coordinate
$Re$ - Reynolds number
$T$ - temperature of the nanofluid
$T_\infty$ - ambient temperature
$x$ - axial coordinate
$\bar{x}$ - dimensionless axial coordinate
$u$ - velocity component along x-axis
$U(x)$ - velocity of the external or potential flow
$U_\infty$ - characteristic velocity
$v$ - velocity component along r-axis

**Greek Symbols**
$\alpha$ - thermal diffusivity
$\beta$ - coefficient of thermal expansion
$\phi$ - nanoparticle volume fraction
$\gamma$ - curvature parameter
$\eta$ - similarity variable
$\lambda$ - mixed convection or buoyancy parameter
$\mu$ - dynamic viscosity
$\nu$ - kinematic viscosity

$\theta$ - dimensionless temperature
$\rho$ - density
$\tau_w$ - wall skin friction
$\psi$ - streamline function

**Subscripts**
$f$ - fluid
$nf$ - nanofluid
$s$ - solid
$w$ - wall

# 1 Introduction

The enhancement in thermal conductivity of conventional fluids via suspensions of solid particles is a modern development in engineering technology aimed at increasing the coefficient of heat transfer. The thermal conductivity of solid metals is higher than the base fluids, so the suspended particles are able to increase the thermal conductivity and heat transfer performance. Choi and Eastman [1] were probably the first researchers to combine a mixture of nanoparticles and base fluid, which they subsequently termed a *nanofluid*. Experimental results [2-7] have illustrated that the thermal conductivity of nanofluid can be increased between 10-50% via introduction of a small volume fraction of nanoparticles. Nanofluidsoffer many diverse advantages in industrial application such as microelectronics, fuel cell, nuclear reactors, biomedicine and transportation, many of which have been reviewed by Wang and Leon [8]. Hwang *et al.* [9] measured the thermal conductivities of various nanofluids and showed that the volume fraction of suspended particle is the effective parameter in enhancing the thermal conductivity. Several numerical studies of nanofluids dynamics have been reported including laminar mixed convection inside horizontal and inclined tubes in which the nanofluid is simulated as a single phase homogeneous mixtures [10,11].

Most nonlinear equations, which are used to describe physical systems in the form of mathematical modeling, do not yield exact solutions. One can solve these nonlinear equations by using numerical or analytical methods. Semi-analytical methods offer certain advantages in comparison with the numerical methods, and one such technique, the Homotopy analysis method (HAM) is used in the present investigation to solve nonlinear differential equations. HAM was introduced into applied mathematics by Liao [12-15] and

employed successfully to produce a general analytic solution strategy for nonlinear problems. HAM has further been employed in other nonlinear problems [16-19], confirming the validity of this method. HAM has also been employed recently used to solve some of nonlinear problems in nanofluid dynamics. Interesting investigations in this regard include Mustafa *et al.* [20] who studied the steady boundary-layer flow and heat transfer near the stagnation-point of a nanofluid towards a stretching sheet. Bég and Tripathi [21] examined the peristaltic propulsion of nanofluids in channels using the Buongiornio formulation and *Mathematica* software. Hassani *et al.* [22] investigated thermo-convective boundary-layer flow of a nanofluid past a stretching sheet. Bég *et al.*[23] studied Brownian motion and thermophoretic effects on mixed convection of nanofluids in porous media using an optimized finite difference scheme. Rana *et al.* [24] recently presented the first finite element simulation of nanofluid convection from an inclined surface with applications in solar energy collector systems.

In the present article, we derive semi-analytical solutions for axisymmetric laminar mixed convection boundary-layer flow past a vertical cylinder in a nanofluid with HAM. Newtonian thermal boundary layers along a vertical cylinder were investigated for a viscous fluid ($\phi = 0$, regular fluid) by Mahmood and Merkin [25]. More recently this problem was extended to a nanofluid by Grosan and Pop [26] numerically. Similarity transformations are employed to render the nonlinear dimensional partial differential boundary layer equations into set of ordinary differential equations, which are solved with HAM. In the current study, we study in detail the influence of nanoparticle volume fraction, curvature parameter and mixed convection (buoyancy) parameter on the dimensionless velocity and temperature profiles, skin frictions and wall temperature gradients.

## 2 Mathematical model

In this article, we assume the steady axisymmetric mixed convection boundary-layer flow along a vertical circular cylinder of radius $a$ immersed in a nanofluid. It is supposed that the mainstream velocity is $U(x)$, the temperature of the cylinder is $T_w(x)$ and the temperature of the ambient nanofluid is $T_\infty$. According to these assumptions and using the Tiwari-Das nanofluid model [27], the governing conservation equations take the form [26]:

$$\frac{\partial}{\partial x}(ru) + \frac{\partial}{\partial r}(rv) = 0 \tag{1}$$

$$u\frac{\partial u}{\partial x}+v\frac{\partial u}{\partial r}=U\frac{dU}{dx}+\frac{\mu_{nf}}{\rho_{nf}}\left(\frac{\partial^2 u}{\partial r^2}+\frac{1}{r}\frac{\partial u}{\partial r}\right)+\frac{\phi\rho_s\beta_s+(1-\phi)\,\rho_f\beta_f}{\rho_{nf}}g\,(T-T_\infty) \tag{2}$$

$$u\frac{\partial T}{\partial x}+v\frac{\partial T}{\partial r}=\alpha_{nf}\left(\frac{\partial^2 T}{\partial r^2}+\frac{1}{r}\frac{\partial T}{\partial r}\right) \tag{3}$$

where $x$ and $r$ are the Cartesian coordinates measured in the axial and radial directions, $u$ and $v$ are the velocity components along $x$ and $r$ directions, respectively. The boundary conditions are prescribed as follows:

$$\begin{aligned} &u=v=0, \quad T=T_w(x)=T_\infty+\Delta T(x/l) \quad at \quad r=a \\ &u=U(x)\to U_\infty(x/l), \qquad T\to T_\infty \text{ as } r\to\infty \end{aligned} \tag{4}$$

The viscosity $\mu_{nf}$, the thermal diffusivity $\alpha_{nf}$ and the thermal conductivity $k_{nf}$ of the nanofluid are defined following Oztop and Abu-Nada[28] as:

$$\begin{aligned} &\mu_{nf}=\tfrac{\mu_f}{(1-\phi)^{2.5}}, \qquad \alpha_{nf}=\tfrac{k_{nf}}{(\rho C_p)_{nf}}, \\ &(\rho C_p)_{nf}=(1-\phi)\,(\rho C_p)_f+\phi\,(\rho C_p)_s \\ &k_{nf}=k_f\frac{(k_s+2k_f)-2\phi\,(k_s-k_f)}{(k_s+2k_f)+\phi\,(k_s-k_f)} \end{aligned} \tag{5}$$

where $(\rho C_p)_{nf}$ is the heat capacitance of the nanofluid. The expression of $\mu_{nf}$ is in accordance with the model proposed by Brinkman [29]. Equation (5) is confined to the case of *spherical nanoparticles* and therefore other geometrical configurations of nanoparticles are not considered in this model. The thermophysical properties of the base fluid (water) and nanoparticles ($Cu$) are presented in Table 1 [28]. Proceeding with analysis, following Grosan and Pop [26], we adopt similarity transformations for eqs. (1)-(3) subject to the boundary conditions (4), in the form:

$$\begin{aligned} &\eta=\frac{r^2-a^2}{2\nu_f l}\left(U_\infty\nu_f l/a^2\right)^{1/2}, \\ &\psi=\left(U_\infty\nu_f a^2/l\right)^{1/2} x\,f\,(\eta)\,, \\ &T-T_\infty=\Delta T\,(x/l)\,\theta\,(\eta) \end{aligned} \tag{6}$$

Table 1: *Thermophysical properties of the base fluid and the nanoparticles*

| Physical properties | Fluid phase (water) | Cu |
|---|---|---|
| $C_p(J/kgK)$ | 4179 | 385 |
| $\rho(kg/m^3)$ | 997.1 | 8933 |
| $k(W/mK)$ | 0.613 | 400 |
| $\alpha \times 10^7(m^2/s)$ | 1.47 | 1163.1 |
| $\beta \times 10^{-5}(1/K)$ | 21 | 1.67 |

where $\psi$ is the dimensional stream function in which $u = (1/r)\partial\psi/dr$ and $v = -(1/r)\partial\psi/dx$

Implementing transformations (6) in (2) and (3), continuity is satisfied and the resulting pair of nonlinear ordinary differential equations is generated:

$$\frac{1}{(1-\phi)^{2.5}\left(1-\phi+\phi\rho_s/\rho_f\right)}\left[(1+2\gamma\eta)\,f'''+2\,\gamma\,f''\right]+ff''$$

$$+1-f'^2+\frac{(1-\phi)+\phi\left(\rho_s/\rho_f\right)\left(\beta_s/\beta_f\right)}{(1-\phi)+\phi\left(\rho_s/\rho_f\right)}\lambda\theta=0, \quad (7)$$

$$\frac{1}{\Pr}\frac{k_{nf}/k_f}{(1-\phi)+\phi(\rho C_p)_s/(\rho C_p)_f}\left[(1+2\gamma\eta)\,\theta''+2\,\gamma\,\theta'\right]+f\theta'-f'\theta=0. \quad (8)$$

The transformed boundary conditions now take the form:

$$f(0)=f'(0)=0, \qquad \theta(0)=1,$$
$$f'(\eta)\to 1, \qquad \theta(\eta)\to 0 \quad as \quad \eta\to\infty \quad (9)$$

where $\Pr = \nu_f/a_f$ is the Prandtl number, $\lambda = Gr/R\ \mathrm{e}^2$ is the mixed convection parameter, $\gamma = \left(\nu_f l/U_\infty a^2\right)^{1/2}$ is the curvature parameter and primes denote to differentiation with respect to $\eta$. Also $Gr = g\beta_f\Delta T\, l^3/v_f^2$ is the Grashof number and $Re = U_\infty l/v_f$ is the Reynolds number. It is pertinent to note that $\lambda < 0$ corresponds to a *cooled cylinder* (opposing

flow), $\lambda = 0$ corresponds to *forced convection flow* ($T_w = T_\infty$) and $\lambda > 0$ corresponds to a *heated cylinder* (assisting flow).

The skin friction coefficient $C_f$ and the Nusselt number $Nu$ are also engineering parameters of interest and are introduced as:

$$C_f = \frac{\tau_w}{\rho_f U_\infty^2}, \qquad Nu = \frac{l q_w}{k_f \Delta T}, \tag{10}$$

where $\tau_w = \mu_{nf} \left(\partial u/dr\right)_{r=a}$ is the skin friction or the shear stress at the surface of the cylinder and $q_w = -k_f \left(\partial T/\partial r\right)_{r=a}$ is the heat flux from the surface of the cylinder. By substituting (5) into (10) and according to the above definitions, we arrive [26] at the following expressions:

$$Re^{1/2} C_f = \frac{\bar{x}}{(1-\phi)^{2.5}} f''(0), \qquad Re^{-1/2} Nu = \frac{k_{nf}}{k_f} \bar{x} \left[-\theta'(0)\right]. \tag{11}$$

## 3 HAM semi-analytical solutions

According to the boundary conditions (9), we select theappropriate initial approximations (for more details, see [12]) as follows:

$$f_0(\eta) = \eta \left(1 - e^{-\eta}\right), \tag{12}$$

$$\theta_0(\eta) = e^{-\eta}, \tag{13}$$

The auxiliary linear operators $\ell_1(f)$ and $\ell_2(\theta)$ are chosen as:

$$\ell_1(f) = f''' + f'', \tag{14}$$

$$\ell_2(\theta) = \theta'' + \theta' \tag{15}$$

with the following properties:

$$\ell_1 \left(c_1 e^{-\eta} + c_2 + c_3 \eta\right) = 0, \tag{16}$$

$$\ell_2 \left(c_4 e^{-\eta} + c_5\right) = 0, \tag{17}$$

where $c_i, i = 1 - 5$, are the arbitrary constants. Due to Eqs. (7)-(8), the

nonlinear operators are:

$$\begin{aligned} N_1\left[\hat{f}(\eta;p),\hat{\theta}(\eta;p)\right] &= \frac{1}{(1-\phi)^{2.5}\left(1-\phi+\phi\rho_s/\rho_f\right)} \\ &\times\left[(1+2\gamma\eta)\frac{\partial^3\hat{f}(\eta;p)}{\partial\eta^3}+2\,\gamma\frac{\partial^2\hat{f}(\eta;p)}{\partial\eta^2}\right] \\ &+\hat{f}(\eta;p)\frac{\partial^2\hat{f}(\eta;p)}{\partial\eta^2}+1-\left(\frac{\partial\hat{f}(\eta;p)}{\partial\eta}\right)^2 \\ &+\frac{(1-\phi)+\phi\left(\rho_s/\rho_f\right)\left(\beta_s/\beta_f\right)}{(1-\phi)+\phi\left(\rho_s/\rho_f\right)}\lambda\hat{\theta}(\eta;p), \end{aligned} \tag{18}$$

$$\begin{aligned} N_2\left[\hat{f}(\eta;p),\hat{\theta}(\eta;p)\right] &= \frac{1}{\Pr}\frac{k_{nf}/k_f}{(1-\phi)+\phi(\rho C_p)_s(\rho C_p)_f} \\ &\times\left[(1+2\gamma\eta)\frac{\partial^2\hat{\theta}(\eta;p)}{\partial\eta^2}+2\,\gamma\frac{\partial\hat{\theta}(\eta;p)}{\partial\eta}\right] \\ &+\hat{f}(\eta;p)\frac{\partial\hat{\theta}(\eta;p)}{\partial\eta}-\frac{\partial\hat{f}(\eta;p)}{\partial\eta}\hat{\theta}(\eta;p). \end{aligned} \tag{19}$$

The *zero-order deformation equations* are composed as:

$$(1-p)\,\ell_1\left[\hat{f}(\eta;p)-f_0(\eta)\right]=p\hbar H_f(\eta)\,N_1\left[\hat{f}(\eta;p),\hat{\theta}(\eta;p)\right], \tag{20}$$

$$(1-p)\,\ell_2\left[\hat{\theta}(\eta;p)-\theta_0(\eta)\right]=p\hbar H_\theta(\eta)\,N_2\left[\hat{f}(\eta;p),\hat{\theta}(\eta;p)\right], \tag{21}$$

subject to the boundary conditions:

$$\begin{aligned} &\hat{f}(0;p)=0, \qquad \frac{\partial\hat{f}(0;p)}{\partial\eta}=0, \qquad \hat{\theta}(0;p)=1, \\ &\frac{\partial\hat{f}(\infty;p)}{\partial\eta}=1, \qquad \hat{\theta}(\infty;p)=0. \end{aligned} \tag{22}$$

For $p\in[0,1]$, we obtain

$$\begin{aligned} &\hat{f}(\eta;0)=f_0(\eta), \qquad \hat{f}(\eta;1)=f(\eta), \\ &\hat{\theta}(\eta;0)=\theta_0(\eta), \qquad \hat{\theta}(\eta;1)=\theta(\eta). \end{aligned} \tag{23}$$

We emphasize that when $p$ increases from 0 to 1, $\hat{f}(\eta;p)$ and $\hat{\theta}(\eta;p)$ vary from $f_0(\eta)$ and $\theta_0(\eta)$ to $f(\eta)$ and $\theta(\eta)$. By Taylor's theorem, finally, we have:

$$\hat{f}(\eta;p) = f_0(\eta) + \sum_{m=1}^{\infty} f_m(\eta)\, p^m, \tag{24}$$

$$\hat{\theta}(\eta;p) = \theta_0(\eta) + \sum_{m=1}^{\infty} \theta_m(\eta)\, p^m, \tag{25}$$

where

$$f_m(\eta) = \frac{1}{m!}\left.\frac{\partial_m \hat{f}(\eta;p)}{\partial p^m}\right|_{p=0}, \qquad \theta_m(\eta) = \frac{1}{m!}\left.\frac{\partial_m \hat{\theta}(\eta;p)}{\partial p^m}\right|_{p=0}. \tag{26}$$

The convergence of the series (24)-(25) strongly depends on the *auxiliary* parameter [12]. Considering that $\hbar$ is selected such that the above series are convergent at $p=1$, then due to Eq.(23) we obtain:

$$f(\eta) = f_0(\eta) + \sum_{m=1}^{\infty} f_m(\eta), \tag{27}$$

$$\theta(\eta) = \theta_0(\eta) + \sum_{m=1}^{\infty} \theta_m(\eta), \tag{28}$$

The $m^{th}$*-order deformation equations* are produced by differentiating Eqs.(20)-(21) $m$ times with respect to $p$, and subsequently dividing by $m!$ in $p=0$, The results now become:

$$\ell_1\left[f_m(\eta) - X_m f_{m-1}(\eta)\right] = \hbar\, H_f(\eta)\; R_{1,m}(\eta), \tag{29}$$

$$\ell_1\left[\theta_m(\eta) - X_m \theta_{m-1}(\eta)\right] = \hbar\, H_\theta(\eta)\; R_{2,m}(\eta), \tag{30}$$

where

$$
\begin{aligned}
R_{1,m}(\eta) = & \frac{1}{(1-\phi)^{2.5}\left(1-\phi+\phi\rho_s/\rho_f\right)} \\
& \times\left[(1+2\gamma\eta)\frac{\partial^3 f_{m-1}(\eta)}{\partial\eta^3}+2\,\gamma\frac{\partial^2 f_{m-1}(\eta)}{\partial\eta^2}\right]+1 \\
& +\sum_{n=0}^{m-1}\left(f_n(\eta)\frac{\partial^2 f_{m-1-n}(\eta)}{\partial\eta^2}-\frac{\partial f_n(\eta)}{\partial\eta}\frac{\partial f_{m-1-n}(\eta)}{\partial\eta}\right) \\
& +\frac{(1-\phi)+\phi\left(\rho_s/\rho_f\right)\left(\beta_s/\beta_f\right)}{(1-\phi)+\phi\left(\rho_s/\rho_f\right)}\lambda\theta_{m-1}(\eta),
\end{aligned}
\tag{31}
$$

$$
\begin{aligned}
R_{2,m}(\eta) = & \frac{1}{\Pr}\frac{k_{nf}/k_f}{(1-\phi)+\phi(\rho C_p)_s/(\rho C_p)_f} \\
& \times\left[(1+2\gamma\eta)\frac{\partial^2\theta_{m-1}(\eta)}{\partial\eta^2}+2\,\gamma\frac{\partial\theta_{m-1}(\eta)}{\partial\eta}\right] \\
& +\sum_{n=0}^{m-1}\left(f_n(\eta)\frac{\partial\theta_{m-1-n}(\eta)}{\partial\eta}-\frac{\partial f_n(\eta)}{\partial\eta}\theta_{m-1-n}(\eta)\right),
\end{aligned}
\tag{32}
$$

and

$$
X_m=\begin{cases}0, & m\le 1,\\ 1, & m\ge 1,\end{cases}
\tag{33}
$$

with the following boundary conditions:

$$
\begin{aligned}
& f_m(0)=0, \qquad f'_m(0)=0, \qquad \theta_m(0)=1, \\
& f'_m(\infty)=1, \qquad \theta_m(\infty)=0.
\end{aligned}
\tag{34}
$$

Finally, we select the followed auxiliary functions

$$
H_f(\eta)=e^{-\eta}, \qquad H_\theta(\eta)=e^{-\eta},
\tag{35}
$$

The symbolic software *MATHEMATICA* is employed to solve the system of linear equations numerically i.e. Eqs.(29)-(30) with the boundary conditions (34), systematically, one after the other, in the order of $m$ = 1,2,3...

## 4 Convergence of HAM

As expounded before, the convergence of the series of Eqs. (27)-(28) effectively depends on the auxiliary parameter. It is imperative to select a proper value of auxiliary parameter to control the rate of convergence of the approximation series – this is achieved with the assistance of the so-called $\hbar-$ curve. It is evident that the valid regions of $\hbar$ correspond to the *straight line segments* nearly parallel to the horizontal axis. This aspect has also been elucidated recently by Tripathi *et al.* [30], Bég*et al.*[31] and Rashidi*et al.* [32] in rheological flow simulations with *HAM*. The different types of $\hbar-$ curve of $f''(0)$ and $\theta'(0)$ obtained by the $20^{th}$-order approximation are illustrated in Figs. 1-2. In order to obtain the optimal value of $\hbar$, the residual errors are

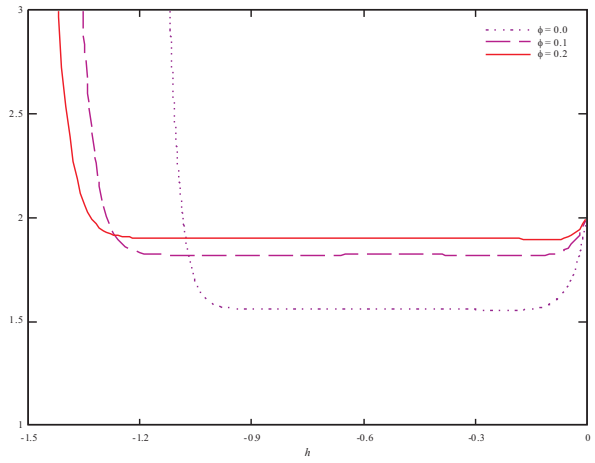


Figure 1: *The h-curve of* $f''(0)$ *obtained by the* $20^{th}$*-order approximation of the HAM solution for different values of nanoparticle volume fraction when* $\gamma = 1$ *and* $\lambda = -0.5$.

documented in Eqs.(36)-(37). These residual errors for the $20^{th}$-order HAM approximation solutions are depicted in Figs. 3-4. Finally, a comparison has been done between the results of present study with the results of previously published data of Ref.[26] for the reduced skin friction coefficient and reduced Nusselt number for different values of the flow parameters in Table 2, showing very good correlation.

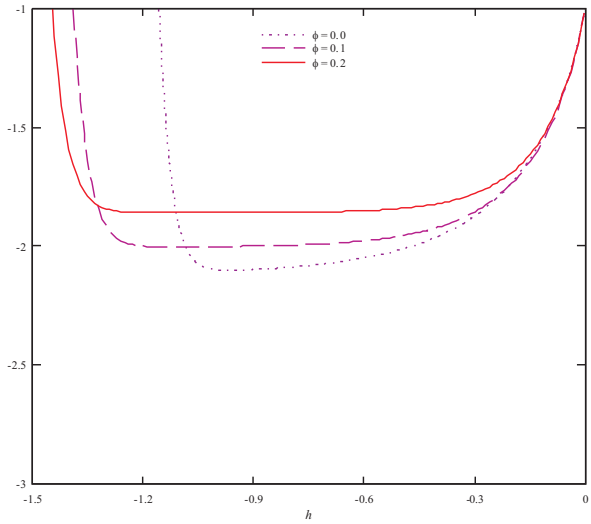


Figure 2: *The h-curve of* $\theta'(0)$ *obtained by the* $20^{th}$*-order approximation of the HAM solution for different values of nanoparticle volume fraction when* $\gamma = 1$ *and* $\lambda = -0.5$.

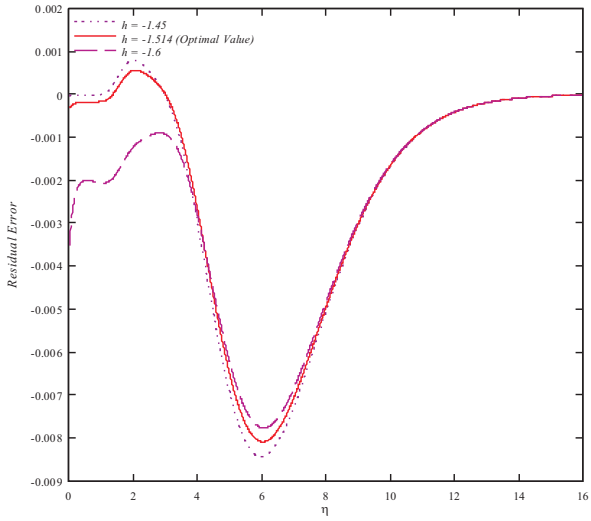


Figure 3: *The residual errors for Eq.(36) using* $20^{th}$*-order of approximations when* $\gamma = \lambda = 0$ *and* $\phi = 0.2$.

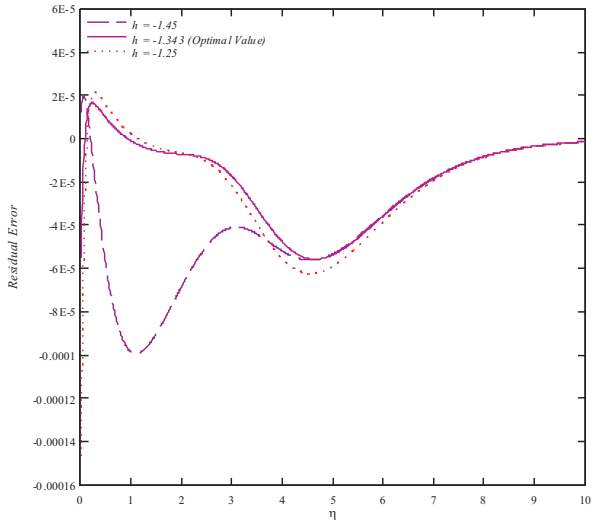


Figure 4: *The residual errors for Eq.(37) using* $20^{th}$*-order of approximations when* $\gamma = 1,\ \lambda = 2$ *and* $\phi = 0.2$.

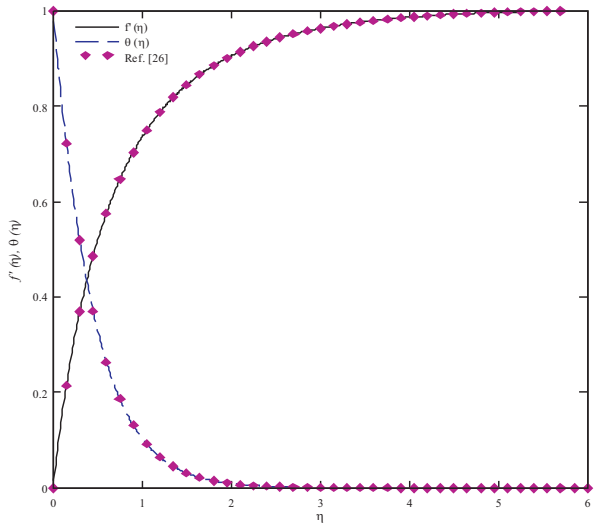


Figure 5: *Verification of* $f'(\eta)$ *and* $\theta(\eta)$ *obtained by* $20^{th}$*-order of HAM solution in comparison with the previously published data of Grosan and Pop [26] when* $\phi = \lambda = 0$ *and* $\gamma = 1$.

Table 2: *Comparison between the results of present study with the results reported by Grosan and Pop [26] for the reduced skin friction coefficient and reduced Nusselt number for different values of the physical parameters*

| $\lambda$ | $\gamma$ | $\frac{f''(0)}{(1-\phi)^{2.5}}$ | | | | $-\frac{k_{nf}}{k_f}\theta'(0)$ | | | |
|---|---|---|---|---|---|---|---|---|---|
| | | $\phi = 0$ | | $\phi = 0.2$ | | $\phi = 0$ | | $\phi = 0.2$ | |
| | | Present | Ref. [26] | Present | Ref. [26] | Present | Ref. [26] | Present | Ref. [26] |
| 0 | 0 | 1.232745 | 1.232587 | 2.622880 | 2.622743 | 1.573414 | 1.573432 | 2.349162 | 2.349363 |
| | 1 | 1.707501 | 1.707622 | 3.469894 | 3.468290 | 2.151547 | 2.151733 | 3.269354 | 3.269380 |
| 1 | 0 | 1.526181 | 1.526774 | 2.916513 | 2.918305 | 1.653432 | 1.652418 | 2.406184 | 2.406390 |
| | 1 | 1.992748 | 1.992152 | 3.756788 | 3.756995 | 2.213481 | 2.213616 | 3.315331 | 3.315332 |

$$
\begin{aligned}
Res_f = & \frac{1}{(1-\phi)^{2.5}\left(1-\phi+\phi\rho_s/\rho_f\right)} \\
& \times \left[(1+2\gamma\eta)\,\frac{d^3 f(\eta)}{d\eta^3} + 2\,\gamma\,\frac{d^2 f(\eta)}{d\eta^2}\right] + 1 \\
& + f(\eta)\,\frac{d^2 f(\eta)}{d\eta^2} - \left(\frac{df(\eta)}{d\eta}\right)^2 \\
& + \frac{(1-\phi)+\phi\left(\rho_s/\rho_f\right)\left(\beta_s/\beta_f\right)}{(1-\phi)+\phi\left(\rho_s/\rho_f\right)}\lambda\theta(\eta)\,,
\end{aligned}
\tag{36}
$$

$$
\begin{aligned}
Res_\theta = & \frac{1}{\Pr}\frac{k_{nf}/k_f}{(1-\phi)+\phi(\rho C_p)_s\,(\rho C_p)_f} \\
& \times \left[(1+2\gamma\eta)\,\frac{d^2\theta(\eta)}{d\eta^2} + 2\,\gamma\frac{d\theta(\eta)}{d\eta}\right] \\
& + f(\eta)\,\frac{d\theta(\eta)}{d\eta} - \frac{df(\eta)}{d\eta}\theta(\eta)\,.
\end{aligned}
\tag{37}
$$

## 5 Results and discussion

In order to measure the accuracy of our results, we compare them with the purely numerical computations of Grosan and Pop [26]. Excellent correlation is observed in Fig.5 between the analytic results obtained by the $20^{th}$-order approximation of *HAM* and numerical results of [26]. In our computations, we have considered a single geometry and material for the nanoparticle, namely Copper (spherical nano-particles), with water as the base fluid. The Prandtl number is prescribed as 6.2 (for water) [28].

The effects of nanoparticle volume fraction variations on the dimensionless velocity and temperature profiles for the case of forced convection flow ($\lambda = 0$) are displayed in Figs.6-7. As the values of the nanoparticles in the base fluid increase, the momentum boundary-layer thickness increases. The boundary layer flow is concomitantly accelerated as observed by the elevation in $f'(\eta)$ profiles. Velocity is clearly minimized for the purely base fluid case

($\phi = 0$) . The presence of nano-particles is therefore beneficial to flow development along the cylinder in the buoyant regime. Figure 6 also demonstrates that with increasing curvature parameter ($\gamma$) , the flow is generally decelerated i.e. velocity function is reduced. In consistency with Mahmmod and Merkin [25] and also Grosan and Pop [26], the flow is *maximized* for the *vertical plate scenario* (vanishing curvature of the cylinder i.e. $\gamma = 0$). For strong curvature of the vertical cylinder ($\gamma = 5$), the flow is decelerated, in particular at increasing values of $\eta$. By increasing the *concentration* of nanoparticles in the base fluid i.e. nano-particle volume fraction ($\phi$), as elucidated earlier, there is also an increase the thermal conductivity and thismanifests with an enhancement in temperatures, as observed in figure 6. Again we note that the purely base fluid (absence of nanoparticles ($\phi = 0$) corresponds to the lowest value of temperature. Furthermore, we note temperature profiles converge faster in the case of a vertical plate ($\gamma = 0$) than the strong curvature vertical cylinder case ($\gamma = 5$) for all the values of the nano-particle volume fraction. The effect on magnitudes of temperature of an increase in curvature parameter is however opposite to the effect sustained by velocity profiles. For the vertical plate case (zero curvature), temperatures are significantly depressed further into the boundary layer regime (i.e. with increasing transverse coordinate, $\eta$), whereas with strong curvature they are enhanced.

Figs.8-9 illustrate the effects of curvature parameter ($\gamma$), on dimensionless velocity and temperature profiles for the case of a *heated cylinder* (assisted flow, $\lambda > 0$). The results show that there is a point near the cylinder wall where the velocity attains the same value for all values of the curvature parameter i.e. velocity ($f'(\eta)$) profiles converges asymptotically to this point. As indicated also in figure 6, the effect of increasing curvature is to significantly decelerate the boundary layer flow i.e. reduce velocity magnitudes. This trend is quickly reached in close proximity to the cylinder surface. Figure 9 reveals that temperature ($\theta(\eta)$) also decays to a location close to the cylinder wall as we progress into the boundary layer. However, with *increasing* curvature, temperatures are generally elevated and this will affect thermal boundary layer thickness very differently from momentum boundary layer thickness. The maximum temperatures correspond to *maximum curvature* parameter ($\gamma = 5$) and vice versa for *the zero curvature* scenario i.e. vertical plate, ($\gamma = 0$).

The effects of mixed convection parameter variations on the dimensionless velocity and temperature profiles are illustrated in Figs.10-11. The changes in the mixed convection parameter consist of three physical cases: assisting

flow (heated cylinder, $\lambda > 0$), opposing flow (cooled cylinder, $\lambda < 0$) and forced convection flow ($\lambda = 0$). The results display that for increasing positive values of the mixed convection parameter, $\lambda$, the flow (fig 10) is strongly accelerated throughout the boundary layer i.e. for all distances transverse to the vertical cylinder. Conversely for increasingly negative values of $\lambda$, the flow is strongly decelerated. The parameter $\lambda = Gr/Re^2$ is directly proportional to Grashof number, $Gr = g\beta_f \Delta T\, l^3/v_f^2$ and this dimensionless number embodies the relative effects of buoyancy force and viscous hydrodynamic force. For $\lambda > 0$,the flow is assisted by buoyancy forces which enhance the momentum boundary layer development and accelerate the flow. The converse effect is sustained for $\lambda < 0$ (where buoyancy force is reversed in direction and inhibits the flow- this leads to retardation in the flow and a plummet in velocities. Furthermore, we note that for any value of $\lambda$ studied, the velocity profiles neither intersect nor do they attain negative values. Back flow i.e. reversal in flow is therefore never instigated in the boundary layer regime. The intermediate case of $\lambda = 0$, corresponds to vanishing buoyancy forces i.e. pure forced convection, and as expected the velocity profile for this scenario falls between that for assisted and opposed flow in Fig.10. Fig.11 shows that increasing mixed convection parameter positively (i.e. $\lambda > 0$) induces the contrary effect on temperature compared with velocity. For $\lambda > 0$ temperatures are significantly depressed in the boundary-layer regime. This is attributable to the elevation in thermal conduction, which is associated with the cylinder surface being heated – thermal energy is drawn from the boundary layer and this manifests in a reduction in the temperatures *inside* the boundary layer. For $\lambda < 0$ the cylinder surface is cooled and as a result, thermal energy is transported via thermal conduction heat transfer into the boundary layer. This effectively accentuates temperatures in the boundary layer as witnessed in figure 11. Buoyancy is therefore a key force influencing flow and heat transfer in the nanofluid. It is as influential as the nano-particle concentration effect, described earlier.

Figs.12-13 depict the distributions of wall skin friction coefficient $f''(0)$ and the wall Nusselt number $\theta'(0)$ for all the thermophysical parameters i.e. buoyancy parameter ($\lambda$), curvature parameter ($\gamma$) and nanoparticle volume fraction ($\phi$). It can be seen that as the nanoparticle volume fraction, curvature parameter and mixed convection parameter increase, the wall skin friction coefficient increases. These parameters therefore clearly accelerate the flow along the cylinder surface, as elaborated earlier. The results also display that the magnitude of the wall Nusselt number increases, as the cur-

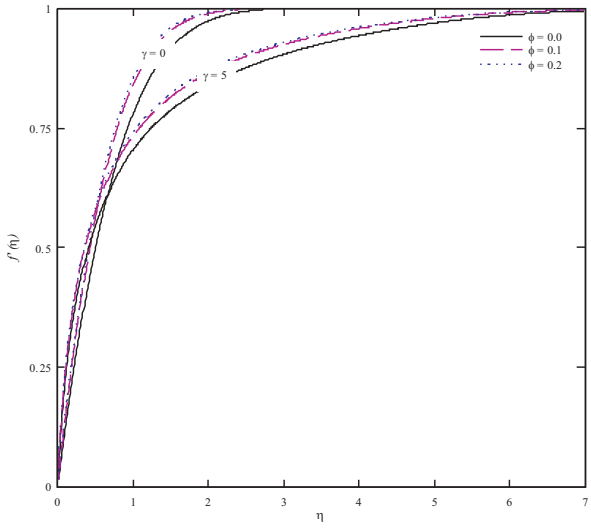


Figure 6: *The effects of nanoparticle volume fraction variations on the dimensionless velocity profiles when* $\lambda = 0$.

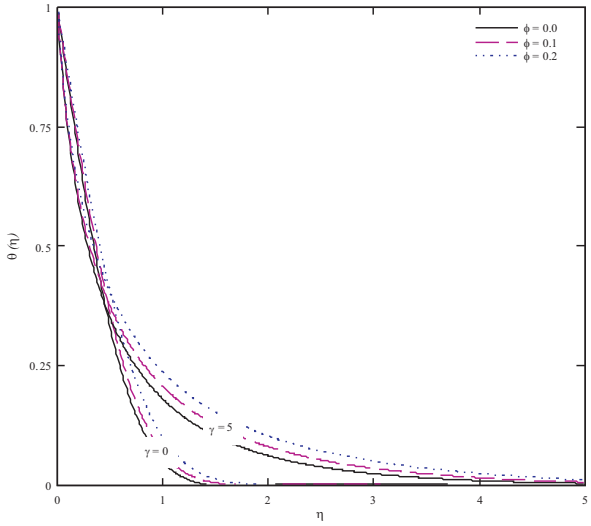


Figure 7: *The effects of nanoparticle volume fraction variations on the dimensionless temperature profiles when* $\lambda = 0$.

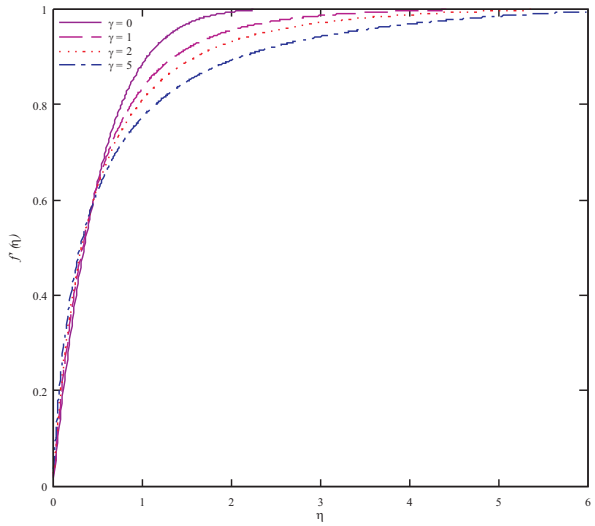


Figure 8: *The effects of curvature parameter variations on the dimensionless velocity profiles when* $\phi = 0.1$ *and* $\lambda = 2$.

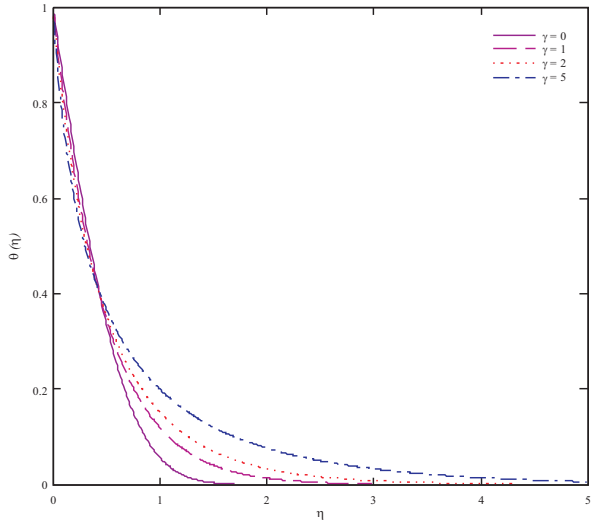


Figure 9: *The effects of curvature parameter variations on the dimensionless temperature profiles when* $\phi = 0.1$ *and* $\lambda = 2$.

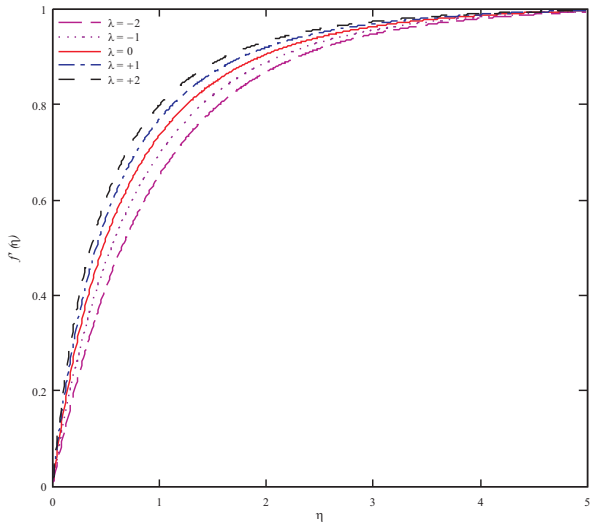


Figure 10: *The effects of mixed convection (buoyancy) parameter variations on the dimensionless velocity profiles when* $\gamma = 1$ *and* $\phi = 0.2$.

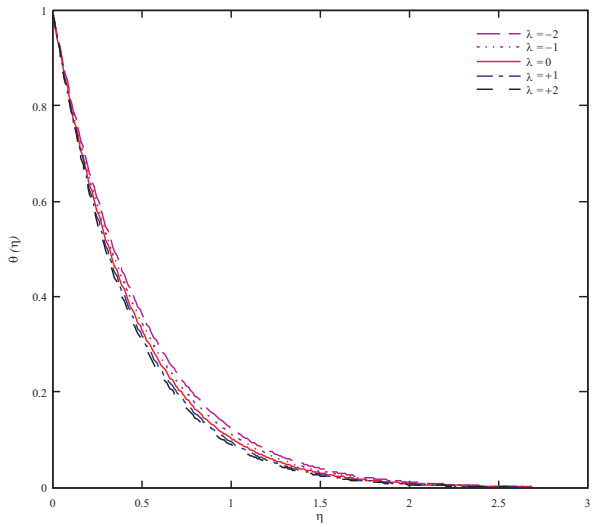


Figure 11: *The effects of mixed convection (buoyancy) parameter variations on the dimensionless temperature profiles when* $\gamma = 1$ *and* $\phi = 0.2$.

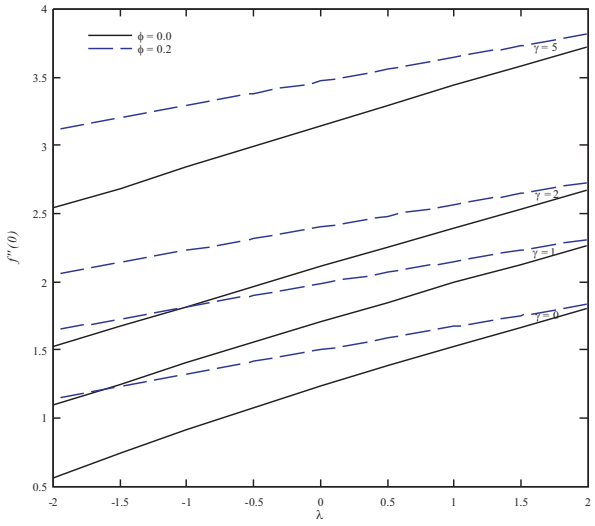


Figure 12: *The variation of skin friction with* $\lambda$ *for different values of the involved parameters.*

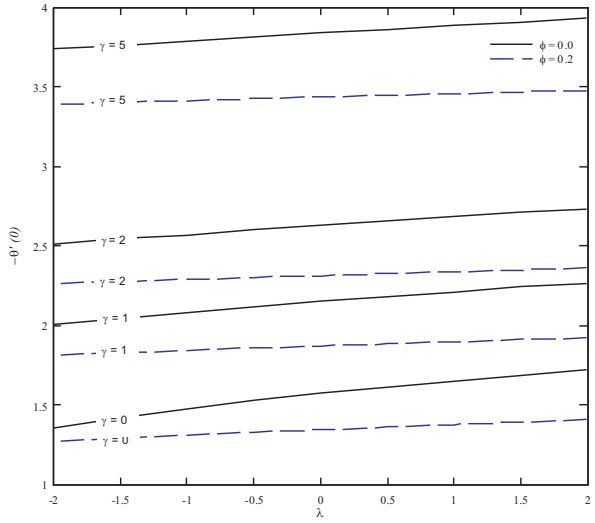


Figure 13: *The variation of wall temperature gradient with* $\lambda$ *for different values of the involved parameters.*

vature parameter or mixed convection parameter increase and conversely wall Nusselt number is depressed with increasing values of nanoparticle volume fraction. In the case of skin friction profiles, the gradient of ascent is steeper however, for the base fluid($\phi = 0$) than for the nanofluid ($\phi = 0.2$) and this trend is maintained for all values of curvature parameter. With regard to wall Nusselt number profiles, a similar response is observed- the gradients of the base fluid profiles are always greater than the corresponding profile for the nanofluid. However, the Nusselt number profiles are inclined less steeply than the skin friction profiles.

## 6 Conclusions

The semi-analytical/numerical technique known as HAM has been implemented to solve the transformed differential equations describing axisymmetric laminar mixed convection boundary-layer flow over a vertical cylinder in a nanofluid. The convergence of the HAM approach has been studied in detail. Benchmarking with previous numerical quadrature solutions has also been conducted. The effects of the three key thermophysicalparameters governing the flow i.e. *nanoparticle volume fraction, curvature parameter* and *mixed convection (buoyancy) parameter* on dimensionless velocity and temperature distributions, skin frictions and wall temperature gradients have been presented graphically and interpreted in detail. The present HAM computations agree closely with previous studies e.g. Grosan and Pop [26]. They further identify that velocity and temperature both increase, with a rise in nanoparticle concentrations i.e. with increasing nano-particle volume fraction. Increasing curvature parameter is found to decelerate the flow but to enhance temperatures. Increasing the mixed convection parameter positively serves to accelerate the flow but acts to decrease temperatures; conversely increasing negative values of mixed convection parameter effectively decelerates the flow but enhances nanofluid temperatures. With an elevation in nanoparticle volume fraction, curvature parameter and mixed convection parameter, the wall skin friction coefficient is strongly elevated. The magnitude of the wall Nusselt number is increased with increasing curvature parameter and mixed convection (buoyancy) parameter and decreasing nanoparticle volume fraction. The present study has considered steady flow only. Future investigations will study *transient* nanofluid convection flows and will be communicated imminently.

# References

[1] S.U.S. Choi, J.A. Eastman, Enhancing thermal conductivity of fluids with nanoparticles, *Materials Science* 231 (1995) 99-105.

[2] H. Masuda, A. Ebata, K. Teramea, N. Hishinuma, Altering the thermal conductivity and viscosity of liquid by dispersing ultra-fine particles, *Netsu Bussei* 4 (1993) 227-233.

[3] S.K. Das, Temperature dependence of thermal conductivity enhancement for nanofluids, *ASME J. Heat Transfer* 125 (2003) 567-574.

[4] B.C. Pak, Y.I. Cho, Hydrodynamic and heat transfer study of dispersed fluids with submicron metallic oxide particles, *Experimental Heat Transfer: AJournal of Thermal Energy* 11 (1998) 151-170.

[5] Y. Xuan, Q. Li, Investigation on Convective Heat Transfer and Flow Features of Nanofluids, *ASME J. Heat Transfer* 125 (2003) 151-155.

[6] J.A. Eastman, S.U.S. Choi, S.Y. Li, W., L.J. Thompson, Anomalously increased effective thermal conductivity of ethylene glycol-based nanofluids containing copper nanoparticles, *Applied Physics Letters* 78 (2001) 718-720.

[7] H.A. Mintsa, G. Roy, C.T. Nguyen, D. Doucet, New temperature dependent thermal conductivity data for water-based nanofluids, *Int. J. Thermal Sciences* 48 (2009) 363-371.

[8] K.V. Wong, O.D. Leon, Applications of nanofluids: current and future, *Advances in Mechanical Engineering* 2010 (2010) 1-12.

[9] K.S. Hwang, J.-H. Lee, S.P. Jang, Buoyancy-driven heat transfer of water-based $Al_2O_3$ nanofluids in a rectangular cavity, *Int. J. Heat and Mass Transfer* 50 (2007) 4003-4010.

[10] M. Akbari, A. Behzadmehr, Developing mixed convection of a nanofluid in a horizontal tube with uniform heat flux, *Int. J. Numerical Methods for Heat and Fluid Flow* 17 (2007) 566 - 586.

[11] M. Akbari, A. Behzadmehr, F. Shahraki, Fully developed mixed convection in horizontal and inclined tubes with uniform heat flux using nanofluid, *Int. J. Heat and Fluid Flow* 29 (2008) 545-556.

[12] S.J. Liao, *Beyond Perturbation: Introduction to the Homotopy Analysis Method*, Chapman & Hall/CRC, Florida, USA (2004).

[13] S.J. Liao, Comparison between the homotopy analysis method and homotopy perturbation method, *Applied Mathematics and Computation* 169 (2005) 1186–1194.

[14] S.J. Liao, On the homotopy analysis method for nonlinear problems, *Applied Mathematics and Computation* 147 (2004) 499-513.

[15] S.J. Liao, An explicit, totally analytic approximation of Blasius viscous flow problems, *Int. J. Non-Linear Mechanics* 34 (1999) 759-778.

[16] M.M. Rashidi, S.A. Mohimanian Pour, T. Hayat, S. Obaidat, Analytic approximate solutions for steady flow over a rotating disk in porous medium with heat transfer by homotopy analysis method, *Computers & Fluids* 54 (2012) 1-9.

[17] M.M. Rashidi, S.A. Mohimanian Pour, Analytic approximate solutions for unsteady boundary-layer flow and heat transfer due to a stretching sheet by homotopy analysis method, *Nonlinear Analysis. Modelling and Control* 15 (2010) 83–95.

[18] M.M. Rashidi, G. Domairry, S. Dinarvand, Approximate solutions for the Burger and regularized long wave equations by means of the homotopy analysis method, *Communications in Nonlinear Science and Numerical Simulation* 14 (2009) 708-717.

[19] S. Husnain, A. Mehmood, O. Anwar Bég and A. Ali, Suction and blowing effects on heat transfer phenomena in unsteady flow through porous media with variable viscosity, *J. Porous Media,* 15 (2012), 293-302.

[20] M. Mustafa, T. Hayat, I. Pop, S. Asghar, S. Obaidat, Stagnation-point flow of a nanofluid towards a stretching sheet, *Int. J. Heat and Mass Transfer* 54 (2011) 5588-5594.

[21] O. Anwar Bég and D. Tripathi, Mathematica simulation of peristaltic pumping with double-diffusive convection in nanofluids: a bio-nano-engineering model,*Proc. IMechE Part N: J. Nanoengineering and Nanosystems* 225, (2012) 99–114.

[22] M. Hassani, M. Mohammad Tabar, H. Nemati, G. Domairry, F. Noori, An analytical solution for boundary layer flow of a nanofluid past a stretching sheet, *Int. J. Thermal Sciences* 50 (2011) 2256-2263.

[23] O. Anwar Bèg, R.S.R. Gorla, V. R. Prasad, B.Vasu and Rana D. Prashad. Computational study of mixed thermal convection nanofluid flow in a porous medium, *Invited paper, $12^{th}$ UK National Heat Transfer Conference, $30^{th}$ August-$1^{st}$ September, Chemical Engineering Department, University of Leeds, UK.* (2011).

[24] P. Rana, R. Bhargava and O.Anwar Bég, Numerical solution for mixed convection boundary layer flow of a nanofluid along an inclined plate embedded in a porous medium, *Computers and Mathematics with Applications,* 64 (2012) 2816–2832.

[25] T. Mahmood, J.H. Merkin, Similarity solutions in axisymmetric mixed-convection boundary-layer flow, *J. Engineering Mathematics* 22 (1988) 73-92.

[26] T. Grosan, I. Pop, Axisymmetric mixed convection boundary layer flow past a vertical cylinder in a nanofluid, *Int. J. Heat and Mass Transfer* 54 (2011) 3139-3145.

[27] R.K. Tiwari, M.K. Das, Heat transfer augmentation in a two-sided lid-driven differentially heated square cavity utilizing nanofluids, *Int. J. Heat and Mass Transfer* 50 (2007) 2002-2018.

[28] H.F. Oztop, E. Abu-Nada, Numerical study of natural convection in partially heated rectangular enclosures filled with nanofluids, *Int. J. Heat and Fluid Flow* 29 (2008) 1326-1336.

[29] H.C. Brinkman, The viscosity of concentrated suspensions and solutions, *J. Chemical Physics* 20 (1952) 571.

[30] D. Tripathi, O. Anwar Bég and J. Curiel-Sosa, Homotopy semi-numerical simulation of peristaltic flow of generalised Oldroyd-B fluids with slip effects, *Computer Methods in Biomechanics Biomedical Engineering* (2012).**DOI:10.1080/10255842.2012.688109**

[31] O. Anwar Bég, M.M. Rashidi, T. A. Bég and M. Asadi, Homotopy analysis of transient magneto-bio-fluid dynamics of micropolar squeeze film in a porous medium: a model for magneto-bio-rheological lubrication, *J. Mechanics in Medicine and Biology,* 12 (2012), 1250051.1-1250051.21.

[32] M.M. Rashidi, O. Anwar Bég and M.T. Rastegari, A study of non-Newtonian flow and heat transfer over a non-isothermal wedge using the Homotopy Analysis Method, *Chemical Engineering Communications,* 199 (2012) 231-256.

Submitted in June 2012., revised in October 2012.

## Homotopska simulacija osnosimetrične mešovite konvekcije u graničnom sloju nanofluida koji teče preko vertikalnog cilindra

Semianalička-numerička tehnika poznata kao metoda homotopske analize ($HAM$) je primenjena na izvodjenje rešenja za laminarno osnosimetričnu mešovitu konvekciju graničnog sloja nanofluida koji teče preko vertikalnog cilindra. Rešenja slicnosti su primenjena na transformaciju paraboličnih parcijalnih diferencijalnih jednačina konzervacije u sistem nelinearnih spregnutih običnih diferencijalnih jednačina, izložen odgovarajućim graničnim uslovima. Za proveru dobijenih rezultata ucinjeno je uporedjenje sa *čisto numeričkim* rezultatima Grosana i Popa (2011) s postignutom odličnom korelacijom. Grafički je ilustrovan učinak zapreminske koncentracije nano čestica, parametra zakrivljenosti i mjeovite konvekcije ili parametra uzgona na distribuciju bezdimenzionalne brzine i temperature, trenja na zidu i zidne gradijente temperature. Utvrdjeno je da HAM pokazuje izvrsnu sposobnost simulacije dinamičkih problema nanofluida. Primena studije uključuje materijale u procesnoj tehnici kao i toplotno poboljšanje energetskih sistema.

doi:10.2298/TAM1204365R Math.Subj.Class.: 82D80, 76E06